Research Article | Vol. 28, No. 7 / 30 March 2020 / Optics Express 9082

Optics EXPRESS

Multifocal microlens arrays using multilayer photolithography

SANG-IN BAE, KISOO KIM, SUNGPYO YANG, KYUNG-WON JANG, AND KI-HUN JEONG*

Department of Bio and Brain Engineering, and KAIST Institute for Health Science and Technology, Korea Advanced Institute of Science and Technology (KAIST), 291 Daehak-ro, Yuseong-gu, Daejeon 34141, South Korea

*kjeong@kaist.ac.kr

Abstract: We report a new microfabrication method of multifocal microlens arrays (MF-MLAs) for extended depth-of-field (DoF) using multilayer photolithography and thermal reflow. Microlenses of different focal lengths were simultaneously fabricated on a single glass wafer by using repeated photolithography with multiple photomasks to define microposts of different thicknesses and concurrent thermal reflow of multi-stacked microposts. The diverse lens curvatures of MF-MLAs are precisely controlled by the thickness of the micropost. Hexagonally packaged MF-MLAs clearly show three different focal lengths of 249 µm, 310 µm, and 460 µm for 200 µm in lens diameter and result in multifocal images on a single image sensor. This method provides a new route for developing various three-dimensional (3D) imaging applications such as light-field cameras or 3D medical endoscopes.

© 2020 Optical Society of America under the terms of the OSA Open Access Publishing Agreement

1. Introduction

Microlens arrays (MLAs) have many benefits of compactness and large field-of-view (FOV) thanks to their short effective focal length and high lens curvature [1,2]. The inherent nature of MLAs allows advanced three-dimensional (3D) imaging [3,4] or security cameras [5]. MLAs are actively being applied for 3D medical endoscopy [6] or light-field imaging [7], using parallax in two different micro images. However, conventional MLAs for 3D imaging have a single focal distance, which confines the depth-of-field (DoF). Microlenses of wide DoF and low numerical aperture (NA) capture in-focus images at multiple depths, which may hinder the accurate depth estimation [8], whereas those of narrow DoF and high NA obtain high spatial resolution. This trade-off substantially holds back 3D camera imaging with extended DoF, which can be resolved by multifocal MLAs [9].

MLAs are conventionally fabricated by using resist reflow [10], inkjet printing [11,12], grayscale lithography [13], or replica molding [14,?]. Unlike other methods, the resist reflow serves as a key method for the wafer-level microfabrication of MLAs [?] and also facilitates the incorporation of diverse fabrication methods for new functions such as aspherical lens curvature [?], high NA [?], antireflection [?], or multi-focus [?]. This method often utilizes a thermoplastic and positive-tone photoresist such as AZ-series or Shipley S1800-series [?]. However, conventional resist exhibits some intrinsic limitations in fabricating multifocal MLAs due to the breakage of photo-crosslinking and the solvent dissolution during multilayer photolithography [?]. Recently, multifocal MLAs of relatively large lens diameters with low NA have been demonstrated by using the guided resist reflowing method, which still has technical limitation in achieving high NA for high spatial resolution [?].

Here we report a novel microfabrication method for fabricating multifocal microlens arrays (MF-MLAs) with extended DoF. This method allows diverse microlenses of high-to-low NA to achieve simultaneously high spatial resolution as well as accurate depth estimation. MF-MLAs can be fabricated at a wafer level by using concurrent thermal reflow of multi-stacked microposts

#388921 https://doi.org/10.1364/OE.388921
Journal © 2020 Received 22 Jan 2020; revised 25 Feb 2020; accepted 5 Mar 2020; published 16 Mar 2020

after defined by repeating photolithography. A thermoplastic and negative tone photoresist serves as a base lens material of MF-MLAs. Like conventional resist reflow method, the lens parameters of MF-MLAs can be precisely controlled by the total thickness and the diameter of multi-stacked microposts. MF-MLAs can not only display multifocal images from microlenses of different focal lengths but also effectively extend the DoF for 3D imaging.

2. MF-MLAs microfabrication

The microfabrication of MF-MLAs was done by using multilayer photolithography of DNR photoresist (DNR L-4615, Dong-jin Semichem. Co., Ltd, Korea) with different photomasks and concurrent thermal reflow of multi-stacked microposts [Figs. 1(a) and 1(b)]. The DNR is an alkaline developable chemical amplification negative photoresist, consisting of phenol-formaldehyde molecules [?]. The DNR resist exhibits both thermoplastic and UV curable properties from its molecular composition, which substantially reduces solvent dissolution and photoresist absorption during multilayer spin-coating [?]. For more details on the microfabrication, a 4-in borosilicate glass wafer was cleaned in piranha solution (5:1 H_2SO_4/H_2O_2) and dehydrated in an oven at 200 °C for 30 mins, followed by HMDS treatment as an adhesion promoter. Three different photomasks of PM1 with all opened patterns, PM2 with 2 opened and 1 closed patterns, and PM3 with 1 opened and 2 closed patterns allow forming multi-stacked microposts with three different thicknesses [Fig. 1(b)]. The first DNR layer was spin-coated and soft-baked at 100 °C for 120 secs for solvent removal. UV light was exposed at 16 mW using the PM1 and then performed post exposure bake (PEB) at 110 °C for 90 secs. The second DNR layer was

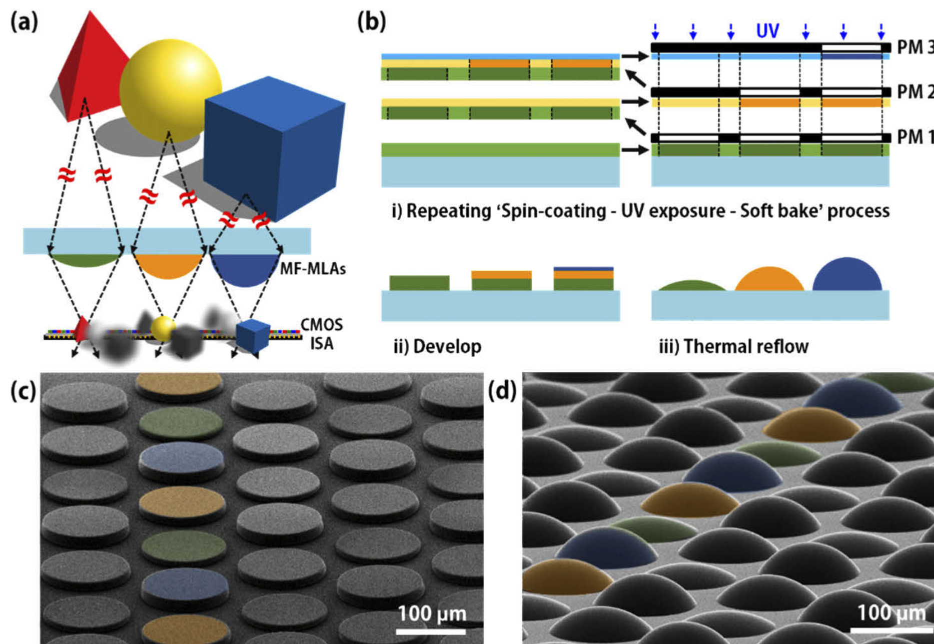

Fig. 1. (a) Schematic illustration of multifocal microlens arrays (MF-MLAs). Objects at different positions are imaged into single CMOS image sensor arrays (CMOS ISA) by MF-MLAs. (b) Microfabrication steps: Repeat 'spin-coating – UV exposure – soft bake' process using different photomasks (PM1, PM2, and PM3), develop and thermal reflow the multi-stacked microposts. (c) Scanning electron microscope (SEM) images of multi-stacked microposts with 3-different thicknesses. Different pseudo colors indicate different micropost thicknesses, and (d) MF-MLAs, after thermally reflow the microposts.

Optics EXPRESS

spin-coated on the first layer. The PM2 was precisely aligned to the pre-defined DNR patterns. After repeating of 'spin-coating – UV exposure – bake' sequences, multi-stacked microposts of different thicknesses were fully developed from the DNR multilayer in TMAH 2.38% aqueous solution concurrently. Finally, MF-MLAS have been successfully fabricated after thermal reflow of the microposts at 140 °C for 30 mins in a convection oven. The SEM images clearly show the multi-stacked microposts of 10, 15, and 20 µm in thicknesses and MF-MLAs (lens diameter of 120 µm) packaged in hexagonal arrays at a constant gap of 25 µm [Figs. 1(c) and 1(d)].

The reflectance, transmittance, and absorbance for a thin DNR layer (26 µm in thickness) on a borosilicate glass wafer were measured in the wavelength range of 450–700 nm [Fig. 2(a)]. The spectral properties indicate that the DNR layer has high transmittance over 0.8 at 550 nm or longer in wavelength. Spin-coating thicknesses were measured on both glass substrate and DNR film [Fig. 2(b)]. The DNR thickness directly controls the lens curvature and the focal length of microlenses. Note that the DNR thickness spin-coated on DNR film is on average 1.56 times higher than that on glass substrate at the same spin-coating speed. The experimental results are

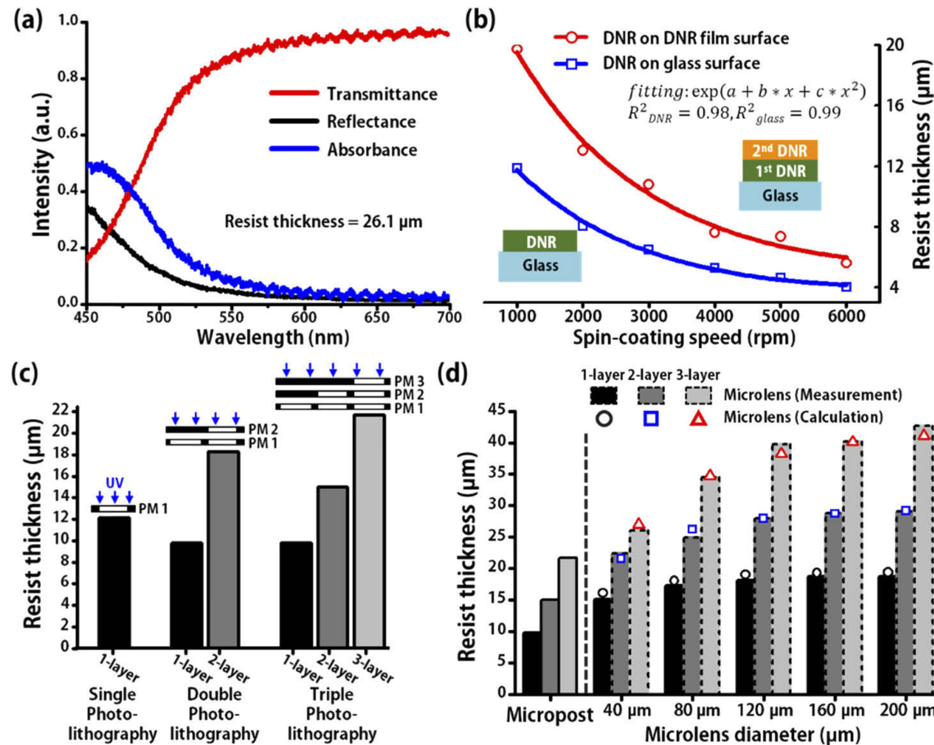

Fig. 2. (a) Reflectance, transmittance, and absorbance of DNR photoresist in the wavelength range of 450–700 nm. (b) Spin-coated DNR thicknesses on glass surface (blue square symbols) and DNR film surface (red circle symbols). The spin-coated thickness of DNR resist on the DNR film surface exhibits on average 1.56 times higher than that on the glass surface. (c) Thicknesses of multi-stacked microposts from multilayer photolithography (single, double, and triple photolithography) by using PM1, PM2, and PM3. Multilayer photolithography reduces the thickness of spin-coated DNR layer by on average 23% during spin-coating and resist baking processes. (d) Thicknesses of multi-stacked microposts and MF-MLAs according to the microlens diameter after thermal reflow. The measurements (gray bars with short dash lines) correspond well with the calculations (rectangle, circle, and triangle symbols).

fitted to a non-linear exponential equation, and R-squared values of each fitted line are 0.98 and 0.99, respectively. Resist thicknesses of each micropost were measured to analyze the thickness variation of multi-stacked microposts depending on the number of multilayer photolithography [single, double, and triple photolithography in Fig. 2(c)]. The resist thickness is slightly reduced after repeating spin-coating and soft-bake processes. The first DNR layer is spin-coated at 1,000 rpm for 30 secs, and both the second and third layers are spin-coated at 6,000 rpm for 30 secs. The thickness of 1-layer in single photolithography, 12 µm in thickness, is different from those of 1-layer in double and triple photolithography. However, the 1-layer thicknesses in both double and triple photolithography are equal to each other at 9.5 µm. At the same time, the thickness of 2-layer in double photolithography, 18.5 µm in thickness, reduces to 14.5 µm in triple photolithography. Regardless of the repetition number of photolithography, the reduction in thickness is 23% on average, which results from the solvent dissolution while repeating spin-coating and resist baking processes. The thicknesses of multi-stacked microposts were compared with those of corresponding MF-MLAs after thermal reflow [Fig. 2(d)]. Black, dark gray, and light gray bars on the left indicate 1-layer, 2-layer, and 3-layer micropost thicknesses from triple photolithography. The same color bar with short dash line on the right represents the corresponding MF-MLAs thickness according to the microlens diameter. Considering the microlens volumes before and after thermal reflow are conserved after sufficient time of soft bake and post exposure bake, volume relationship equations based on calculations in [**?**] is also applied to thermal reflow of MF-MLAs. The experimental results (bars) correspond well with the calculations (circle, rectangle, and triangle symbols) using the volume relationship equations after thermal reflow. As a result, all the lens parameters such as lens curvature and F-number are simply controlled by the resist thickness and the lens diameter.

3. MLAs characterization

The multifocal properties of MF-MLAs were measured by using a confocal laser scanning microscope (CLSM) with a 533 nm green laser source. Figure 3(a) shows top and cross-sectional confocal images of MF-MLAs for 120 µm in diameter and 25 µm in gap. The cross-sectional image clearly shows different focal lengths ($f_1 = 178$ µm, $f_2 = 130$ µm, and $f_3 = 113$ µm) of MF-MLAs corresponding to the top view. The measured focal lengths [gray bars, Fig. 3(b)] of MF-MLAs are similar to focal lengths calculated from the thickness of microposts [red lines, Fig. 3(b)]. The different gray bars indicate the focal lengths of MF-MLAs reflowed from multi-stacked microposts. The focal length quadratically reduces as the resist thickness increases at lens diameter over 80 µm. However, the focal lengths at 40 µm in lens diameter show intriguing features due to the aspect ratio (AR, a ratio of micropost thickness (t_P) to micropost diameter (D_P), i.e. t_P/D_P) of microposts [Fig. 3(c)]. A concave behavior of focal length curve occurs at 40 µm, which results from the lens shape. The minimum focal length appears exactly as a hemispherical lens shape, when radius of curvature and the lens radius are the same. The microlens reflowed from a micropost with an aspect ratio (AR) of 1/3 generates a hemispherical lens, which a central angle is 180°, and has minimum focal length. In other words, a microlens resulting from a micropost of AR over 1/3 (AR = 0.38, $D_P = 40$ µm and $t_P = 15$ µm) exhibits a hyper hemispherical lens (360° in azimuth angle and over 90° in zenith angle). Note that a hemispherical lens after thermal reflow is theoretically formed at an AR of 1/3, based on the calculation [**?**]. The SEM image shows MF-MLAs of 40 µm in diameter with various ARs (0.25, 0.38, and 0.5) [Fig. 3(d)].

Optics EXPRESS

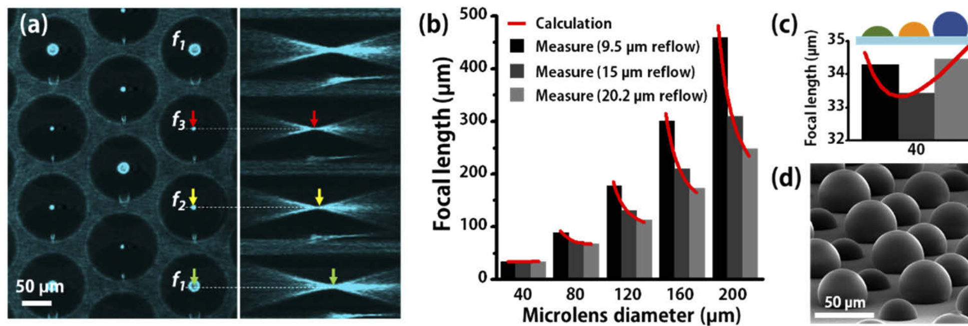

Fig. 3. Multifocal properties of hexagonally packaged MF-MLAs. (a) Top and cross-sectional images of MF-MLAs with 3-different focal lengths ($f_1 = 178$μm, $f_2 = 130$μm, and $f_3 = 113$μm), obtained by confocal line scanning microscope (CLSM) images, microlens diameter of 120 μm. (b) Measured (bars) and calculated (curves) focal lengths of MF-MLAs at 40, 80, 120, 160, and 200 μm in diameters. The different bars (black, gray, light gray) represent the measured focal length of microlens reflowed from microposts of 9.5 μm, 15 μm, and 20.2 μm in thickness, respectively. (c) A concave focal length curve appears at 40 μm in diameter and (d) SEM image of MF-MLAs at 40 μm in diameter with various aspect ratios (ARs) including AR over 1/3.

4. Multifocal arrayed images

Multifocal images from MF-MLAs were clearly captured along x-axis for a target object of 'OPTICS' characters on OLED display of 8 cm x 5 cm at three different magnifications (Fig. 4). The MF-MLAs ($f_1 = 249$ μm, $f_2 = 310$ μm, and $f_3 = 460$ μm at $D_L = 200$ μm) were precisely placed

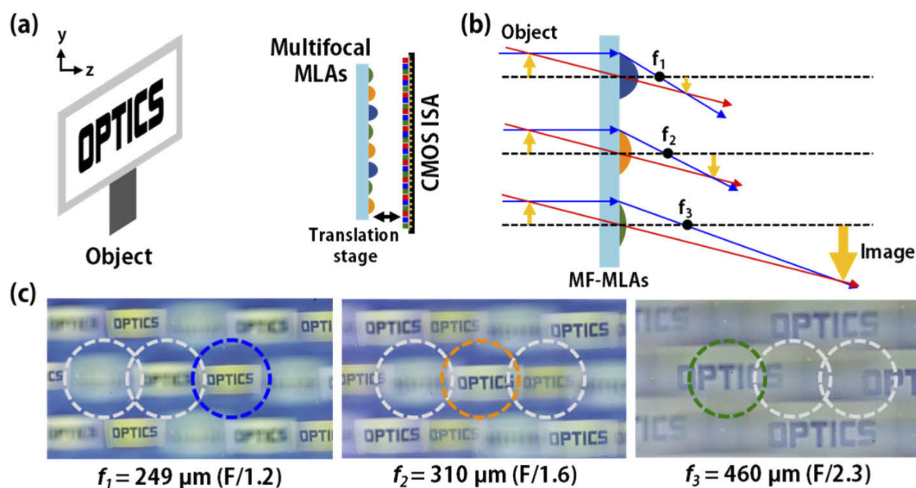

Fig. 4. Captured multifocal images from characters 'OPTICS' at different focal lengths ($f_1 = 249$ μm, $f_2 = 310$ μm, and $f_3 = 460$ μm) by using MF-MLAs of 200 μm in lens diameter. (a) An optical setup for capturing the multifocal images. A target object, MF-MLAs, and a CMOS image sensor arrays (CMOS ISA) were place along x-axis. MF-MLAs were precisely placed to face a CMOS ISA using a xyz translation stage. (b) Image magnification depending on the focal lengths at the same aperture size. (c) Captured CMOS images from different microlenses focal length of f_1, f_2, and f_3. Corresponding F-numbers are 1.2, 1.6, and 2.3, respectively.

to face an 8-megapixel CMOS image sensor arrays (CMOS ISA) (SONY IMX 219, SONY Corp., pixel size = 1.12 μm) using a xyz translation stage. Considering a single pixel size of CMOS ISA, the depth-of-focus values are 5.6 μm, 6.9 μm, and 12.8 μm and their corresponding DoF ranges are 8.0–12.4 mm, 12.3–21.7 mm, and 21.1–49.2 mm for object distances of 10 mm, 16 mm, and 30 mm away from the image sensor, respectively. As a result, the MF-MLAs substantially extend the overall DoF range from 8.0 mm to 49. 2 mm as well as clearly form in-focus images within the DoF range.

5. Conclusion

In summary, this work has successfully demonstrated monolithic fabrication of multifocal microlens arrays (MF-MLAs) for extended depth-of-field. The monolithic fabrication of MF-MLAs was simply done by using multilayer photolithography of DNR resist and thermal reflow of multi-stacked microposts with different thicknesses. Like a conventional resist reflow method, all the lens parameters of MF-MLAs are also precisely controlled by the resist thickness and the lens diameter. Hexagonally packaged MF-MLAs show extended depth-of-field ranges and capture multifocal images at three different magnifications. The MF-MLAs provide a new route for developing arrayed camera for advanced light-field applications such as light-field microscope, automated 3D inspection, or face recognition.

Funding

National Research Foundation of Korea (2019023700); Ministry of Health and Welfare (HI16C1111); Pemtron Co., Ltd..

Disclosures

The authors declare no conflicts of interest.

References

1. K.-H. Jeong, J. Kim, and L. P. Lee, “Biologically inspired artificial compound eyes,” Science **312**(5773), 557–561 (2006).
2. D. Keum, K.-W. Jang, D. S. Jeon, C. S. Hwang, E. K. Buschbeck, M. H. Kim, and K.-H. Jeong, “Xenos peckii vision inspires an ultrathin digital camera,” Light: Sci. Appl. **7**(1), 80 (2018).
3. R. Horisaki, S. Irie, Y. Ogura, and J. Tanida, “Three-dimensional information acquisition using a compound imaging system,” Opt. Rev. **14**(5), 347–350 (2007).
4. S.-H. Hong, J.-S. Jang, and B. Javidi, “Three-dimensional volumetric object reconstruction using computational integral imaging,” Opt. Express **12**(3), 483–491 (2004).
5. Y. M. Song, Y. Xie, V. Malyarchuk, J. Xiao, I. Jung, K.-J. Choi, Z. Liu, H. Park, C. Lu, and R.-H. Kim, “Digital cameras with designs inspired by the arthropod eye,” Nat. Methods **497**(7447), 95–99 (2013).
6. J. Geng and J. J. I. S. J. Xie, “Review of 3-d endoscopic surface imaging techniques,” IEEE Sens. J. **14**(4), 945–960 (2014).
7. R. Ng, M. Levoy, M. Brédif, G. Duval, M. Horowitz, and P. Hanrahan, “Light field photography with a hand-held plenoptic camera,” Computer Science Technical Report CSTR **2**, 1–11 (2005).
8. T. Georgiev and A. Lumsdaine, “The multifocus plenoptic camera,” in *Digital Photography VIII* (International Society for Optics and Photonics, 2012), p. 829908.
9. C. Perwass and L. Wietzke, “Single lens 3d-camera with extended depth-of-field,” in *Human Vision and Electronic Imaging XVII* (International Society for Optics and Photonics, 2012), p. 829108.
10. Z. D. Popovic, R. A. Sprague, and G. N. Connell, “Technique for monolithic fabrication of microlens arrays,” Appl. Opt. **27**(7), 1281–1284 (1988).
11. J. Y. Kim, N. B. Brauer, V. Fakhfouri, D. L. Boiko, E. Charbon, G. Grutzner, and J. Brugger, “Hybrid polymer microlens arrays with high numerical apertures fabricated using simple ink-jet printing technique,” Opt. Mater. Express **1**(2), 259–269 (2011).
12. X. Zhou, Y. Peng, R. Peng, X. Zeng, Y.-A. Zhang, and T. Guo, “Fabrication of large-scale microlens arrays based on screen printing for integral imaging 3d display,” ACS Appl. Mater. Interfaces **8**(36), 24248–24255 (2016).
13. D. Kuang, X. Zhang, M. Gui, and Z. Fang, “Hexagonal microlens array fabricated by direct laser writing and inductively coupled plasma etching on organic light emitting devices to enhance the outcoupling efficiency,” Appl. Opt. **48**(5), 974–978 (2009).

Optics EXPRESS

14. J. Albero, L. Nieradko, C. Gorecki, H. Ottevaere, V. Gomez, H. Thienpont, J. Pietarinen, B. Päivänranta, and N. J. O. e. Passilly, "Fabrication of spherical microlenses by a combination of isotropic wet etching of silicon and molding techniques," Opt. Express **17**(8), 6283–6292 (2009).
15. T. Chung, Y. Lee, S. P. Yang, K. Kim, B. H. Kang, and K. H. Jeong, "Mining the smartness of insect ultrastructures for advanced imaging and illumination," Adv. Funct. Mater. **28**(24), 1705912 (2018).
16. S. Audran, B. Faure, B. Mortini, C. Aumont, R. Tiron, C. Zinck, Y. Sanchez, C. Fellous, J. Regolini, and J. Reynard, "Study of dynamical formation and shape of microlenses formed by the reflow method," in *Advances in Resist Technology and Processing XXIII* (International Society for Optics and Photonics, 2006), p. 61534D.
17. Y. Hu, Y. Chen, J. Ma, J. Li, W. Huang, and J. Chu, "High-efficiency fabrication of aspheric microlens arrays by holographic femtosecond laser-induced photopolymerization," Appl. Phys. Lett. **103**(14), 141112 (2013).
18. H. Jung and K.-H. Jeong, "Monolithic polymer microlens arrays with high numerical aperture and high packing density," ACS Appl. Mater. Interfaces **7**(4), 2160–2165 (2015).
19. S.-I. Bae, Y. Lee, Y.-H. Seo, and K.-H. Jeong, "Antireflective structures on highly flexible and large area elastomer membrane for tunable liquid-filled endoscopic lens," Nanoscale **11**(3), 856–861 (2019).
20. M.-K. Park, H. J. Lee, J.-S. Park, M. Kim, J. M. Bae, I. Mahmud, and H.-R. Kim, "Design and fabrication of multi-focusing microlens array with different numerical apertures by using thermal reflow method," J. Opt. Soc. Korea **18**(1), 71–77 (2014).
21. F. T. O'Neill and J. T. Sheridan, "Photoresist reflow method of microlens production part i: Background and experiments," Optik **113**(9), 391–404 (2002).
22. Y. Hirai, K. Sugano, T. Tsuchiya, and O. Tabata, "A three-dimensional microstructuring technique exploiting the positive photoresist property," J. Micromech. Microeng. **20**(6), 065005 (2010).
23. T. Kim, R. Shin, M. Jung, J. Lee, C. Park, and S. Kang, "Drag reduction using metallic engineered surfaces with highly ordered hierarchical topographies: Nanostructures on micro-riblets," Appl. Surf. Sci. **367**, 147–152 (2016).
24. J. C. Moore, "Successful photoresist removal: Incorporating chemistry, conditions, and equipment," in *Advances in Resist Technology and Processing XIX* (International Society for Optics and Photonics, 2002), pp. 892–903.